Mechanics and Mechanical Engineering
Vol. 21, No. 2 (2017) 389–413

An Original Technique for Modeling of Anisotropic Viscoelasticity of Orthotropic Materials in Finite Element Codes Applied to the Mechanics of Plates and Shells

Volodymir G. Martynenko
Dynamic and Strength of Machines Department
National Technical University
Kharkiv Polytechnic Institute
Kyrpychova str. 2, 61002, Kharkiv, Ukraine
martynenko.volodymyr@gmail.com

Received (10 February 2017)
Revised (12 March 2017)
Accepted (13 April 2017)

The paper presents an original technique for the numerical modeling of temperature dependent anisotropic viscoelastic properties in finite element codes. The study relates to the use of ANSYS Mechanical Student Products 17.2 code, but also is applicable to the other structural finite element codes. The solved one- and two-dimensional problems illustrate a possibility of an adaptation of the proposed combined-material model to the solution of model problems with a sufficient accuracy in comparison with the developed analytical solutions. An estimation of the performance of the technique shows its applicability to solution of the contact problems of orthotropic viscoelasticity of thin shells including multilayered options. The performed practical application of the method to the contact problem of cylindrical shell prove this point.

Keywords: anisotropic viscoelasticity, rheological model, thin shell, Finite Element Method, shift function, relaxation tensor.

1. Introduction

Nowadays composites are widely used as innovative materials in automobile, aviation and aerospace industry, in pipeline repairs, and in energy industry due to their lightweight and high strength properties. The most popular composites are glass and carbon fiber reinforced composites [1]. The mechanical properties of these materials are more complicated in comparison with steel and aluminum ones. Among them, it worth noting the orthotropic elastic and viscoelastic properties due to presence of directed fibers and polymeric matrix [2].

Viscoelasticity is a special property of polymers that is reflected as an increasing displacement under constant loading and decreasing stresses under constant strain because of change of their molecular shapes [3].

Composite materials are stiff enough to keep strains and displacements in a small range. Therefore, a linear viscoelasticity theory can be used to reflect the mechanical behavior of composite constructions in most cases, including contact problems of composite shells [4].

Popular finite-element codes such as ANSYS and ABAQUS include a consideration of a viscoelasticity phenomenon. However, the time and frequency domain applications of viscoelastic properties deal with independent shear and bulk viscoelastic behavior of materials neglecting a difference between viscous properties in different directions i.e. their anisotropy [5, 6]. Elastic properties of materials can still be orthotropic. This means that relaxation curves in different directions according to the current material model are proportional to the initial elastic values. It is a strong requirement that must fit to the appropriate experimental data.

Nevertheless, there is a significant number of situations where a distinction between anisotropy level of elastic and viscoelastic properties should be taken into account. For instance, Shu and Onat in the work [7] first considered a necessity of application of anisotropic viscoelasticity to practical problems and made the main problem formulation. Taylor and co-workers in [8] proved the need of modeling of anisotropic viscoelasticity for biomechanical applications and developed a GPU-based finite element solver for an acceleration of the solution. Nedjar in the paper [9] presented a method for the solution of a finite strain anisotropic viscoelastic model for description of fiber-reinforced composites that represented soft biological tissues. Lubarda and Asaro in [10] applied a theory of anisotropic viscoelasticity to a modeling of the mechanics of biological membranes and presented the solution for the plane stress state case. Santos and co-workers in [11] investigated a wave propagation in transversely isotropic viscoelastic thin plates solving non–coercive elliptic boundary-value problems formulated in the space frequency domain using a Galerkin finite-element procedure.

Bretin and Wahab in [12] showed an applicability of Green functions to the solution of an anisotropic viscoelastic material model. Hwy and Chen in [13] applied a boundary value method to a consideration of anisotropically viscoelastic plane bodies with defects. Bai and Tsavkin in [14] presented the time-domain finite difference algorithm for simulating of the multicomponent data in viscoelastic transversely isotropic media with a vertical symmetry axis.

Lvov and Martynenko in [15] showed an importance of an application of an anisotropic viscoelastic material model to a mechanical behavior of the repair bandage of main pipelines. Also in [16] the authors developed an analytical approach to modeling of orthotropic viscoelasticity for different contacting conditions between a pipeline and a repair bandage.

As it follows from the sources above anisotropic viscoelasticity is a considerable topic but most of the papers does not enable a technique for generalization of this property to the whole number of mechanical constructions. The promising way in this direction is an adaptation of commercial finite lements codes to an accounting of anisotropy of viscoelastic behavior.

Poon and Ahmad in the paper [17] presented a finite element update scheme for an anisotropic viscoelasticity with Schapery–type non–linearity, proposed in the work [18] and its implementation into the finite element code of ABAQUS. Gerngross and Pellegrino in [19] in a similar way adapted a nonlinear viscoelastic material

model proposed by Rand and co–workers for balloons in [20, 21] to the finite element code of the CAE ABAQUS through a user's subroutine. A type of non–linearity of a viscoelastic material for this paper was also defined by Shapery in [18]. Staub and co–workers in [22] developed a numerical scheme of a time integration in an anisotropic viscoelastic domain that represents a composite with inhomogeneously oriented fibers and adapted it to an implementation into the CAE ABAQUS. Cavallini in his paper [23] implemented linear isotropic and anisotropic viscoelasticity into the mathematical package of symbolic computations Mathematica. Liefeith and Kolling in [24] showed an approach to modeling of finite rubber orthotropic viscoelasticity considering an implicit and explicit implementation into the finite element code LS–DYNA with numerical examples that illustrate an adequacy of the proposed method.

In the main, the discussed works consider an implementation of integration schemes into finite element code of ABAQUS, excluding one paper with a LS-DYNA usage. At the same time, there is no any implementation of anisotropic viscoelasticity into the CAE ANSYS Mechanical. However, ANSYS Mechanical is one of the most powerful tools for analyzing of a mechanical behavior and strength of structures [25]. It is connected with a complication of an implementation of time integration schemes into the finite element code of ANSYS in comparison with ABAQUS.

This paper presents the technique for modeling of a linear orthotropic viscoelasticity without usage of complex integration algorithms using the tools, provided by the commercial Finite Element code "by default" considering a developed method. An adequacy of the proposed algorithm is checked using a number of numerical experiments.

2. Simplifications of anisotropic viscoelastic material models

A rheological representation of a linear viscoelastic material behavior in a one–dimensional problem can be reflected as a system of springs with stiffnesses k_e and k_i and damping elements with viscosities μ_i, using a generalized Maxwell model (Fig. 1a).

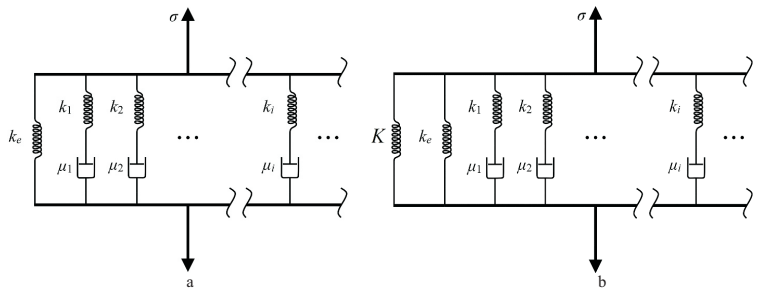

Figure 1 Rheological models of viscoelastic materials: a) one-material model; b) two-material model

For the case of one–dimensional elastic material model it can be represented as a single spring with stiffness K.

Let us combine two material models in parallel (Fig. 1b). This model can be equivalently replaced by the model with $K_e = K + k_e$ as the resulting elastic element stiffness. This case is depicted in Fig. 1a, if one changes k_e symbol to K_e symbol.

According to [4] the Boltzman superposition integral for the resulting system in the case of an absence of a previous loading history is:

$$\sigma(t) = \int_0^t E_{rel}(t-\xi)\frac{d\varepsilon(\xi)}{d\xi}d\xi \tag{1}$$

where: $E_{rel}(t) = K_e + \sum_i k_i \exp(-\frac{\tau_i}{t})$ and $\tau_i = \mu_i/k_i$.

Generalizing Eq. (1) to the multiaxial case we gain:

$$\hat{\sigma}(t) = \int_0^t \hat{R}(t-\xi)\frac{d\hat{\varepsilon}(\xi)}{d\xi}d\xi \tag{2}$$

where $\hat{\sigma}(t)$ is the second range stress tensor, $\hat{\varepsilon}(t)$ is the second range strain tensor, $\hat{R}(t)$ is the fourth range tensor of relaxation kernels.

In a component form Eq. (2) is represented as:

$$\sigma_{lm}(t) = \int_0^t \sum_n \sum_p R_{lmnp}(t-\xi)\frac{d\varepsilon_{np}(\xi)}{d\xi}d\xi \tag{3}$$

Here l, m, n, $p = 1, 2, 3$ for the 3–dimenensional case.

With respect to the form of the expression for $E_{rel}(t)$ the tensor of relaxation kernels can also be generalized to a representation by well-known Prony series:

$$R_{lmnp}(t) = C_{lmnp} + \sum_i \mu^i_{lmnp} \exp(-\frac{t}{\tau^i_{lmnp}}), \tag{4}$$

where C_{lmnp} are the coefficients of the symmetric elastic stiffness tensor.

Using famous rearranging of Eq. (3), presented in [26], and combining it with the expression (4) it can be equivalently represented as:

$$\sigma_{lm}(t) = \sum_n \sum_p C_{lmnp}\varepsilon_{np}(t) - \int_0^t \sum_n \sum_p [\sum_i k^i_{lmnp} \exp(-\frac{t}{\tau^i_{lmnp}})]\varepsilon_{np}(\xi)d\xi \tag{5}$$

where: $k^i_{lmnp} = \frac{\mu^i_{lmnp}}{\tau^i_{lmnp}}$.

And finally:

$$\sigma_{lm}(t) = \sum_n \sum_p C_{lmnp}\{\varepsilon_{np}(t) - \int_0^t [\sum_i a^i_{lmnp} \exp(-\frac{t}{\tau^i_{lmnp}})]\varepsilon_{np}(\xi)d\xi\} \tag{6}$$

where: $a^i_{lmnp} = \frac{k^i_{lmnp}}{C_{lmnp}}$.

The effect of a change of a temperature T on viscoelastic properties for thermorheologically simple materials (TSM) can be accounted changing the real time variable t by the fictitious time $\tilde{t}_{lmnp}$ [27]:

$$\tilde{t}_{lmnp}(T) = \frac{t}{A_{lmnp}(T)} \tag{7}$$

where $A_{lmnp}(T)$ is a temperature-dependent shift function, such that for the reference temperature T_r $A_{lmnp}(T_r) = 1$.

If to postulate a material, in which the viscoelastic properties are proportional to the elastic ones, then:

$$\begin{cases} a^i_{lmnp} = a_i \\ \tau^i_{lmnp} = \tau_i \\ \tilde{t}_{lmnp}(T) = \tilde{t}(T) \end{cases} \tag{8}$$

For the case of isotropic material, one can rearrange (3) to the form:

$$\hat{\sigma}(t) = \int_0^t \hat{G}(t-\xi)\frac{d\hat{e}(\xi)}{d\xi}d\xi + \hat{I}\int_0^t K(t-\xi)\frac{d\Delta(\xi)}{d\xi}d\xi, \tag{9}$$

where $\hat{G}(t)$ and $K(t)$ are the shear relaxation tensor and the bulk relaxation function, $\hat{I}$ is a unity tensor, $\hat{e}(t)$ and $\Delta(t)$ are the deviatoric and volumetric parts of strains.

This equation is a general equation for the representation of viscoelastic material properties in the finite element code of ANSYS Mechanical.

Shear and bulk relaxation kernels are also represented by Prony series [5]:

$$\begin{cases} \hat{G}(t) = \hat{G}_0[a^G_\infty + \sum_i^{n_G} a^G_i \exp(-\frac{t}{\tau^G_i})] \\ K(t) = K_0[a^K_\infty + \sum_i^{n_K} a^K_i \exp(-\frac{t}{\tau^K_i})] \end{cases} \tag{10}$$

where $\hat{G}_0$ and K_0 are the initial shear relaxation moduli tensor and bulk relaxation moduli, n_G and n_K are numbers of Prony terms, a^G_i and a^K_i are relative moduli, a^G_∞ and a^K_∞ are relative moduli on the infinity, τ^G_i and τ^K_i are relaxation times.

Despite the fact that viscoelastic properties in ANSYS are isotropic, elastic ones still can be orthotropic. This situation is correspondent to the case of the relations (6) taking into account (8) and considering C_{lmnp} as components of the stiffness tensor with relations on technical constants that are typical for orthotropic materials [28].

Therefore, ANSYS Mechanical does not enable a consideration of a general case of anisotropy of viscoelastic properties. However, this paper presents a technique for modeling of the more general case of linear orthotropic viscoelasticity using standard tools of ANSYS Mechanical Student Products 17.2 [29].

3. Technique of combined material models

The technique consists in that one builds two identical space domains in the same location. Further we mesh them successively – each domain with its properties (elastic or viscoelastic). Since the algorithm of the mesher operates equally for coincidental domains, the nodes and elements of both meshes coincide with each

other. On the next step one needs to merge all the nodes. Thereby the resulting nodes correspond to the elements of elastic and viscoelastic group at the same time. That is why the whole finite element model will be deformed jointly with their contributions to the energy potential. This means, that the elements of each material group will experience the individual stress state under the same displacement field. The resulting stress tensor field in the model is a sum of stress tensor fields for each group of elements. The scheme of the method is described in Fig. 2.

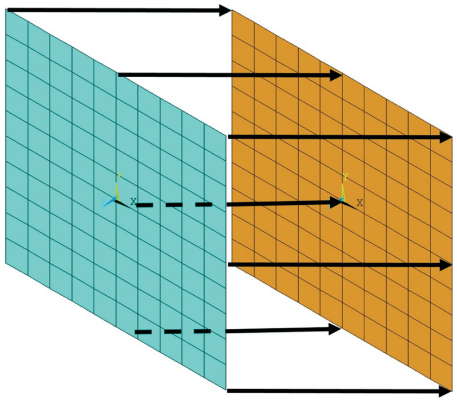

Figure 2 Merging of coincident nodes for elastic (blue) and viscoelastic (orange) finite element models

We postulate, that a single viscoelastic material model is analogous to a combined material model, consisted of portions of elastic and viscoelastic materials, with proper selection of elastic and viscoelastic parameters.

3.1. *One–dimensional test*

To check this assumption let us consider a plane stress problem of stretching of a long thin plate that reflects a creep test. The calculation model for this problem in ANSYS is represented in Fig. 3.

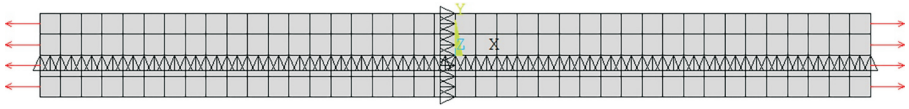

Figure 3 Calculation model for the numerical test

Let us consider four cases – finite element model with one viscoelastic material, finite element model with combined elasto–viscoelastic material and two rheological

spring dashpot model that correspond to Fig. 1a and Fig. 1b, reflected by integral equation (1) with a stress $\sigma(t)$, defined by constant force P = 10^7 N:

$$\int_0^t E_{rel}(t-\xi)\frac{d\varepsilon(\xi)}{d\xi}d\xi = P \tag{11}$$

For the one–material ANSYS test we use the parameters, presented in Tab. 1 (viscoelastic parameters are the same for the shear and bulk parts). For the two–material ANSYS test they are showed in Tab. 2. The spring dashpot model, which correspond to Fig. 1a, was solved with the values, presented in Tab. 3 and the spring dashpot model, which corresponds to Fig. 1b, has the values from Tab. 4. The integral equation (11) for the current number of coefficients of a Prony series was solved, using the mathematical package Maple [30].

Table 1 Input parameters for the one–dimensional one–material test

Material parameter	Designation	Value	Unit
Elastic modulus	$(E)_1$	$2*10^{11}$	Pa
Poisson's ratio	$(\nu)_1$	0	-
Prony series multiplier	$(a)_1$	0.1	-
Relaxation time	$(\tau)_1$	5	s

Table 2 Input parameters for the one–dimensional two–material test

Material parameter	Designation	Value	Unit
Elastic modulus of the elastic material	$(E_1)_2$	$1*10^{11}$	Pa
Poisson's ratio of the elastic material	$(\nu_1)_2$	0	-
Elastic modulus of the viscoelastic material	$(E_2)_2$	$1*10^{11}$	Pa
Poisson's ratio of the viscoelastic material	$(\nu_2)_2$	0	-
Prony series multiplier of the viscoelastic material	$(a_2)_2$	0.2	-
Relaxation time of the viscoelastic material	$(\tau_2)_2$	5	s

It is obvious from (1) that in order to gain a conformity between one–material and two material models the material parameters should satisfy the following conditions: $(\tau)_1 = (\tau_2)_2 = (\tau)_3 = (\tau)_4$, $(k_e)_3 = (K)_4 + (k_e)_4$, $(k_1)_3 = (k_e)_3 * (a)_3$, $(k_1)_4 = (k_e)_4 * (a)_4$, $(E)_1 * (a)_1 = (E_2)_2 * (a_2)_2$, $(E)_1 = (E_1)_2 + (E_2)_2$, $(\nu)_1 = (\nu_1)_2 = (\nu_2)_2$.

Fig. 4a and Fig. 4b show the displacement versus time curves of the end (for the point $x_e = 0.5$ m) of the domain in the spring-dashpot Wiechert model (the third

Table 3 Input parameters for the one–material spring–dashpot model

Material parameter	Designation	Value	Unit
Stiffness of the spring element	$(k_e)_3$	$2*10^{11}$	Pa
Stiffness of the spring-dashpot element	$(k_1)_3$	$2*10^{10}$	Pa
Prony series multiplier	$(a)_3$	0.1	-
Relaxation time	$(\tau)_3$	5	s

Table 4 Input parameters for the two-material spring-dashpot model

Material parameter	Designation	Value	Unit
Stiffness of the spring element of the elastic material	$(K)_4$	$1*10^{11}$	Pa
Stiffness of the spring element of the viscoelastic material	$(k_e)_4$	$1*10^{11}$	Pa
Stiffness of the spring–dashpot element of the viscoelastic material	$(k_1)_4$	$2*10^{10}$	Pa
Prony series multiplier	$(a)_4$	0.2	-
Relaxation time	$(\tau)_4$	5	s

case) and in the finite-element model, built in ANSYS, (the first case) respectively. The analogous curves for the second and fourth cases totally merge with the first and the third ones respectively (because the error cannot be recognized visually for the current graph resolution), so they are not presented.

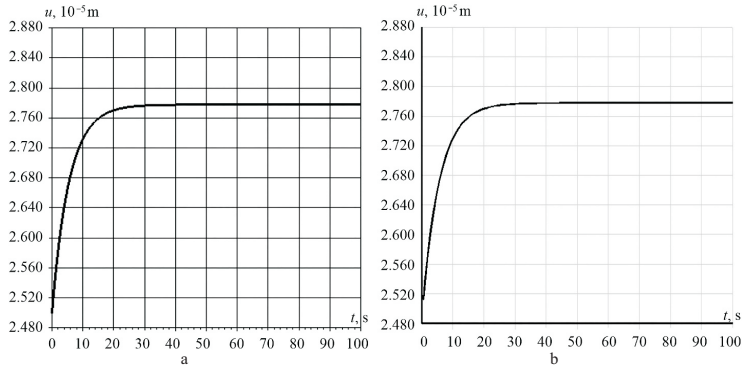

Figure 4 Displacement vs. time curves for the one-dimensional test: a) analytical solution for the Wiechert model, Maple 15 output; b) numerical solution in ANSYS, ANSYS Mechanical POST26 output

The elastic, viscoelastic and total displacements of the ends of one-dimensional models are summarized in Table 5. Here and below the relative error is evaluated as: abs{[*Analytical Solution*]–[*ANSYS Solution*]}/min{[*Analytical Solution*], [*ANSYS Solution*]}.

Table 5 Displacement values and relative errors estimation for the one–dimensional tests

Case		Displacement 10^{-5} m	Relative error %
Analytical solution for the one- and two- material tests	Elastic	2.500	-
	Viscoelastic	0.278	-
	Total	2.778	-
ANSYS solution for the one-material test	Elastic	2.501	< 0.1
	Viscoelastic	0.278	< 0.1
	Total	2.779	< 0.1
ANSYS solution for the two-material test	Elastic	2.501	< 0.1
	Viscoelastic	0.279	0.4
	Total	2.780	< 0.1

As one can see from the figures and table above, elastic and viscoelastic values of the deformations coincide with a very small error for all the cases. It should be emphasized again, that according to the way of defining of viscoelastic material model by equalities (10) in order to reflect the same viscoelastic behavior the relations between elastic moduli and Prony series multipliers must satisfy the following relation:

$$\frac{(E)_1}{(E_2)_2} = \frac{(a_2)_2}{(a)_1}. \tag{12}$$

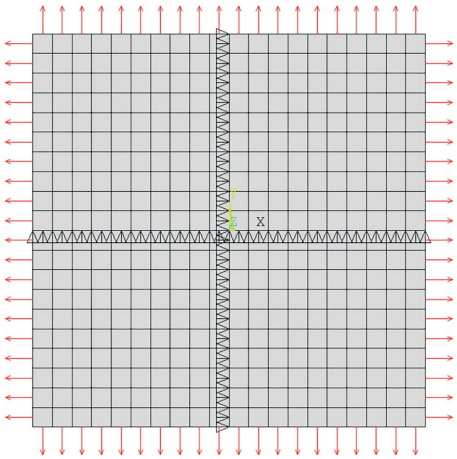

Figure 5 Calculation model for the multi-axial stress state

3.2. *Generalization to the multi-axial stress-strain state*

Let us consider a quadratic thin plate loaded on the perimeter by equal distributed forces $1*10^8$ N/m in both directions, experiencing plane stress state (Fig. 5).

It is possible to obtain an analytical solution for the current boundary-value problem:

$$\frac{\partial \sigma_x}{\partial x} + \frac{\partial \tau_{xy}}{\partial y} + X,\ \frac{\partial \tau_{xy}}{\partial x} + \frac{\partial \sigma_y}{\partial y} + Y \tag{13}$$

$$\begin{cases} \varepsilon_x = S_{11}[\sigma_x(t) + \int_0^t \Pi_{11}(t-\tau)\sigma_x(\tau)d\tau] + S_{12}[\sigma_y(t) \\ + \int_0^t \Pi_{12}(t-\tau)\sigma_y(\tau)d\tau] \\ \varepsilon_y = S_{21}[\sigma_x(t) + \int_0^t \Pi_{21}(t-\tau)\sigma_x(\tau)d\tau] + S_{22}[\sigma_y(t) \\ + \int_0^t \Pi_{22}(t-\tau)\sigma_y(\tau)d\tau] \\ \gamma_{xy} = S_{33}[\tau_{xy}(t) + \int_0^t \Pi_{33}(t-\tau)\tau_{xy}(\tau)d\tau] \end{cases} \tag{14}$$

$$\varepsilon_x = \frac{\partial u}{\partial x} \qquad \varepsilon_y = \frac{\partial v}{\partial y} \qquad \gamma_{xy} = \frac{\partial u}{\partial x} + \frac{\partial v}{\partial y} \tag{15}$$

$$u(0,y,t) = 0 \qquad v(x,0,t) = 0 \qquad \sigma_x(t) = \sigma_y(t) = P \tag{16}$$

where: u and v are the X– and Y–displacements respectively, ε_x, ε_y and γ_{xy} are the directional linear and angular strains respectively, σ_x, σ_y and τ_{xy} are the directional normal and shear stresses respectively, X and Y are body forces, Π_{11}, Π_{22}, Π_{12}, Π_{21} and Π_{33} are the components of a scaled creep rate tensor, represented by Prony series [26], S_{11}, S_{22}, S_{12}, S_{21} and S_{33} are the coefficients of the compliance tensor, which has the proper dependencies on the technical elastic constants [31]:

$$S_{11} = 1/E_x,\ S_{22} = 1/E_y,\ S_{12} = S_{21} = -\nu_{xy}/E_x = -\nu_{yx}/E_y,\ S_{33} = 1/G_{xy} \tag{17}$$

For the constant force boundary conditions (statically indeterminate problem) the Airy stress function can be used to gain the solution of the viscoelastic problem similarly to the elastic one [32]:

$$\varphi(x,y,t) = \frac{k_1}{2}x^2 + k_2 xy + \frac{k_3}{2}y^2 \tag{18}$$

where k_1 and k_3 are normal distributed forces on the Y-constant and X-constant boundaries respectively, k_2 is a shear distributed force on the boundaries.

For the absence of the shear distributed force the displacements are represented by the following integral forms:

$$\begin{cases} u = S_{11}k_3[1 + \int_0^t \Pi_{11}(t-\tau)d\tau]x + S_{12}k_1[1 + \int_0^t \Pi_{12}(t-\tau)d\tau]x \\ v = S_{21}k_3[1 + \int_0^t \Pi_{21}(t-\tau)d\tau]y + S_{22}k_1[1 + \int_0^t \Pi_{22}(t-\tau)d\tau]y \end{cases} \tag{19}$$

Thus, the displacements can be obtained using equalities (19), strains and stresses are gained considering relations (15) and (14) respectively.

Let us now consider numerical simulations of the current problem in ANSYS.

For the first case we take a viscoelastic material with orthotropic elastic properties and viscoelastic properties, which are proportional to the elastic ones. This type of material can be represented using standard ANSYS mechanical tools.

For the second case we take a viscoelastic material with independent orthotropic elastic and viscoelastic properties, i.e. they are not proportional to each other. This type of material can be modeled using the technique presented in the paper. One need to add an orthotropic elastic material and a viscoelastic material, then mesh two coincident domains with different material options and merge coincident nodes.

The material properties for the first case are presented in Tab. 6, and for the second one – in Tab. 7. As it can be seen from the initial data the elastic properties of the second material are several orders of magnitude less than the ones of the first material. This requirement, as well as the requirements to the material parameters, discussed for the one–dimensional test, must be satisfied in order to avoid an influence of the second material on the elastic properties of the resulting combined material.

Table 6 Input parameters for the first two–dimensional one–material test

Material parameter	Designation	Value	Unit
Elastic modulus in X-direction	$(E_x)_1$	$2*10^{11}$	Pa
Elastic modulus in Y-direction	$(E_y)_1$	$1*10^{11}$	Pa
Shear modulus	$(G_{xy})_1$	$1*10^{10}$	Pa
Poisson's ratio	$(\nu_{xy})_1$	0.3	-
Prony series multiplier for the shear relaxation kernel	$(a^G{}_1)_1$	0.2	-
Prony series multiplier for the bulk relaxation kernel	$(a^K{}_1)_1$	0.2	-
Relaxation time for the shear relaxation kernel	$(\tau^G{}_1)_1$	5	s
Relaxation time for the bulk relaxation kernel	$(\tau^K{}_1)_1$	5	s

Also in order to trace the influence of increasing elastic properties of the second material of the combined model on the resulting displacements let them reach the values, presented in Tab. 8.

For one-material two-dimensional test it is possible to plot the X- and Y-displacements versus time curves, gained from the analytical solution according to the equations in (19), for the corner point (x_c = 0.5 m, y_c = 0.5 m), showed in Fig. 6a. Here and further, the X-displacement is reflected by the black curve and the gray one reflects the Y-displacement. The dependence of the X- and Y-displacements of the corner point of the plate on time for one- and two- material tests in ANSYS Mechanical are presented in Fig. 6b and coincide with each other for the appropriate curves.

The curves of the X- and Y-displacements versus time for the case of modified input parameters of the two-material model are presented in Fig. 6c.

It is obvious that an increasing order of magnitude of elastic stiffness tensor coefficients of the second material for the combined material model increases the error.

Table 7 Input parameters for the first two-dimensional two–material test

Material parameter	Designation	Value	Unit
Elastic modulus in X-direction for the elastic material	$(E_{x1})_2$	$2*10^{11}$	Pa
Elastic modulus in Y-direction for the elastic material	$(E_{y1})_2$	$1*10^{11}$	Pa
Shear modulus for the elastic material	$(G_{xy1})_2$	$1*10^{10}$	Pa
Poisson's ratio for the elastic material	$(\nu_{xy1})_2$	0.3	-
Elastic modulus in X-direction for the viscoelastic material	$(E_{x2})_2$	$2*10^{7}$	Pa
Elastic modulus in Y-direction for the viscoelastic material	$(E_{y2})_2$	$1*10^{7}$	Pa
Shear modulus for the viscoelastic material	$(G_{xy2})_2$	1	Pa
Poisson's ratio for the viscoelastic material	$(\nu_{xy2})_2$	0.3	-
Prony series multiplier for the shear and bulk relaxation kernels of the viscoelastic material	$(a^G{}_2)_2$ $(a^K{}_2)_2$	2000	-
Relaxation time for the shear and bulk relaxation kernel of the viscoelastic material	$(\tau^G{}_2)_2$ $(\tau^K{}_2)_2$	5	s

Table 8 Modified parameters for the viscoelastic material in the first two–dimensional two–material test

Material parameter	Designation	Value	Unit
Elastic modulus in X-direction for the viscoelastic material	$(E_{x2})_3$	$2*10^{9}$	Pa
Elastic modulus in Y-direction for the viscoelastic material	$(E_{y2})_3$	$1*10^{9}$	Pa
Shear modulus for the viscoelastic material	$(G_{xy2})_3$	1	Pa
Poisson's ratio for the viscoelastic material	$(\nu_{xy2})_3$	0.3	-
Prony series multiplier for the shear and bulk relaxation kernels of the viscoelastic material	$(a^G{}_2)_3$, $(a^K{}_2)_3$	2000	-
Relaxation time for the shear and bulk relaxation kernel of the viscoelastic material	$(\tau^G{}_2)_3$, $(\tau^K{}_2)_3$	5	s

Thereby an engineer should keep these values as small as possible, increasing in as much time the values of coefficients a_i^G and a_i^K.

As it follows from the figures for the default viscoelastic material model of ANSYS the elastic and viscoelastic properties are proportional to each other. This means that the bigger value of the elastic displacement is, the bigger value of the viscoelastic one becomes. And in addition, this dependence is linear.

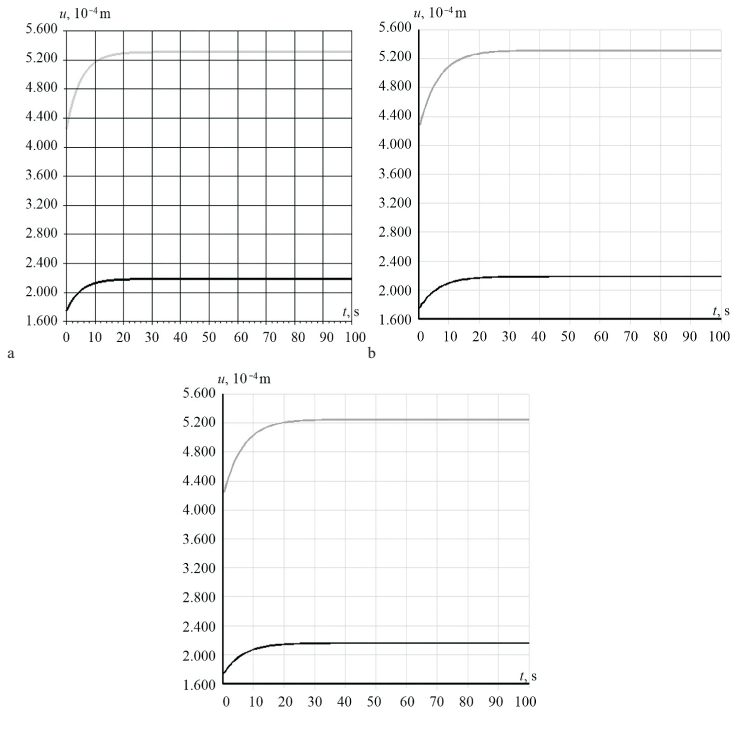

Figure 6 Displacements vs. time curves for the first two–dimensional test: a) analytical solution; b) ANSYS solution for the one–material model and two–material model with optimal parameters; c) ANSYS solution for the two–material model with suboptimal parameters

Let us consider the situation, where the material exhibits viscoelastic phenomenon only in one direction. This case can be a result of unidirectional reinforcement of a soft polymeric matrix by stiff fibers. In order to achieve this one needs to change viscoelastic properties in Y–direction of the second material of the combined material model by changing an appropriate elastic modulus to the value, that is much smaller than X–direction Young modulus, for instance: $(E_{y2})_4 = 1 * 10^4$ Pa. There is no any ability to let the Young modulus reach a zero value due to the positive definiteness of the elastic stiffness tensor. For the analytical model this means that $\Pi_{22}(t) = 0$.

As it follows from the initial data the viscoelastic properties in X-direction still influences on the Y-displacements via Poisson's ratio ν_{xy}.

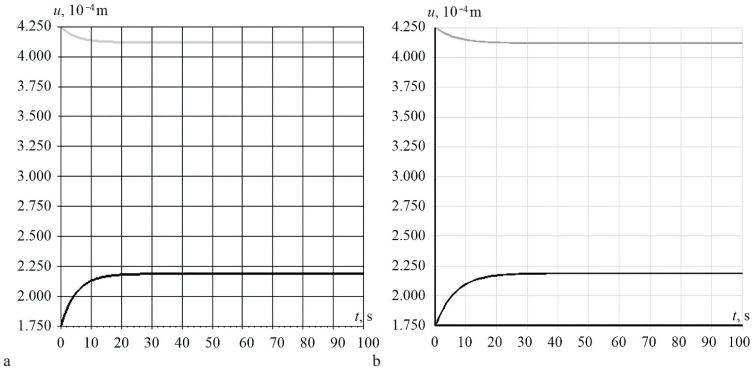

Figure 7 Displacements vs. time curves for the second two–dimensional test: a) analytical solution; b) ANSYS solution for the one–material model and two-material model with optimal parameters

Fig. 7a and Fig. 7b represent the X– and Y–displacements for this case for analytical and numerical solutions respectively.

As it can be seen from the figures, the Y–displacement of the corner point decreases with time due to a non-zero Poisson's coefficient.

The obtained displacement values for the first case with an evaluation of relative errors are summarized in Table 9. Table 10 represents the results for the second case.

This a brief overview of the relative errors in the evaluation of viscoelastic displacements via the proposed combined-material method. The error in evaluation of viscoelastic strains and stresses will be discussed further in this paper.

Table 9 Displacement values and relative errors estimation for the first two-dimensional test

Case		X-disp. 10^{-3} m	Y-disp. 10^{-3} m	Relative error % X–disp.	Y–disp.
Analytical solution	Elastic	0.17500	0.42500	-	-
	Viscoelastic	0.04375	0.10625	-	-
	Total	0.21875	0.53125	-	-
One–material ANSYS test	Elastic	0.17502	0.42505	< 0.1	< 0.1
	Viscoelastic	0.04401	0.10689	0.6	0.6
	Total	0.21903	0.53194	0.1	0.1
Two–material ANSYS test	Elastic	0.17500	0.42500	< 0.1	< 0.1
	Viscoelastic	0.04412	0.10705	0.6	0.7
	Total	0.21912	0.53205	0.1	0.1
Two–material ANSYS test with modified parameters	Elastic	0.17500	0.42500	< 0.1	< 0.1
	Viscoelastic	0.04137	0.10018	6.7	6.3
	Total	0.21637	0.52518	1.3	1.2

Table 10 Displacement values and relative errors estimation for the second two–dimensional test

Case		X-disp. 10^{-3} m	Y-disp. 10^{-3} m	Relative error % X–disp.	Y–disp.
Analytical solution	Elastic	0.17500	0.42500	-	-
	Viscoelastic	0.04375	-0.01313	-	-
	Total	0.21875	0.41188	-	-
Two–material ANSYS test	Elastic	0.17500	0.42500	< 0.1	< 0.1
	Viscoelastic	0.04412	-0.01317	0.6	0.7
	Total	0.21912	0.41217	0.1	0.1

3.3. *Way for accounting of anisotropy of relaxation times*

The method presented in the previous paragraph deals with a type of anisotropic viscoelasticity which does not account differences between relaxation times in different directions and temperature shift functions in different directions, i.e.:

$$\begin{cases} \tau^i_{lmnp} = \tau_i \\ \tilde{t}_{lmnp}(T) = \tilde{t}(T) \end{cases} \tag{20}$$

In order to account this effect, the multimaterial model can be used.

Consider a rearranging of the relaxation kernel tensor $\hat{R}(t)$ in Eq. (2) into the following form:

$$\hat{R}(t) = \sum_l \sum_m \sum_n \sum_p \hat{R}_{lmnp}(t) \tag{21}$$

where $\hat{R}_{lmnp}(t)$ is a tensor with the only one non-zero component $R_{lmnp}(t)$ for the diagonal components and two non-zero components located symmetrically about the tensors diagonal for the nondiagonal components.

Thus (2) will be rewritten:

$$\hat{\sigma}(t) = \sum_l \sum_m \sum_n \sum_p \int_0^t \hat{R}_{lmnp}(t-\xi)\frac{d\hat{\varepsilon}(\xi)}{d\xi}d\xi \tag{22}$$

Eq. (22) can be interpreted as a sum of the following physical relations:

$$(\hat{\sigma}(t))_{lmnp} = \int_0^t \hat{R}_{lmnp}(t-\xi)\frac{d\hat{\varepsilon}(\xi)}{d\xi}d\xi \tag{23}$$

where $(\hat{\sigma}(t))_{lmnp}$ is a stress tensor of one of the fictitious materials of the combined material model.

In this way, it is possible to apply anisotropic viscoelastic properties, including relaxation times and temperature shift functions, to ANSYS for each direction individually:

$$\begin{aligned}(\hat{\sigma}(t))_{lmnp} &= \int_0^{\tilde{t}_{lmnp}} \hat{G}_{lmnp}(\tilde{t}_{lmnp}-\xi)\frac{d\hat{e}(\xi)}{d\xi}d\xi \\ &+\hat{I}\int_0^{\tilde{t}_{lmnp}} K_{lmnp}(\tilde{t}_{lmnp}-\xi)\frac{d\Delta(\xi)}{d\xi}d\xi\end{aligned} \tag{24}$$

$$\begin{cases} \hat{G}_{lmnp}(t) = (\hat{G}_0)_{lmnp}[(a^G_\infty)_{lmnp} + \sum_i^{(n_G)_{lmnp}} (a^G_i)_{lmnp} \exp(-\frac{t}{(\tau^G_i)_{lmnp}})] \\ K_{lmnp}(t) = (K_0)_{lmnp}[(a^K_\infty)_{lmnp} + \sum_i^{(n_K)_{lmnp}} (a^K_i)_{lmnp} \exp(-\frac{t}{(\tau^K_i)_{lmnp}})] \end{cases} \quad (25)$$

where all the coefficients with indexes *lmnp* are defined for the corresponding fictitious material in the corresponding direction.

Thus in order to apply three–dimensional orthotropically viscoelastic material model one needs to define ten materials – one material for the elastic properties and nine materials for the viscoelastic properties in each direction, defined similarly to the combined–material model in Paragraph 3.2 i.e. elastic properties of each material should be several orders of magnitude less in comparison with the elastic material. Finally, the user gains a viscoelastic material with fully independent elastic and viscoelastic properties. Despite the existence of such a possibility defining of this type of material requires a huge number of the experimental data, that's why this model may be used in very special calculations.

3.4. *Visualization of strain and stress results in ANSYS Mechanical APDL*

As it follows from the Cauchy kinematic relations between displacements and strains the strain tensor is fully defined by a displacement vector. Thus the "true" strain distribution can be obtained in the ANSYS Mechanical APDL General Postprocessor and Timehistory Postprocessor by default, visualizing the strain result for one of the materials in the combined material model (for instance, elastic material).

At the same time, it is obvious that each element, which belongs to the same nodes in the combined material model, has its own stress distributions due to the different material properties. If to combine relations (22) and (23), one can gain that the resulting "true" stress is the sum of stresses for all elements in the combined material model:

$$\hat{\sigma}(t) = \sum_l \sum_m \sum_n \sum_p (\hat{\sigma}(t))_{lmnp} \quad (26)$$

That's why the user needs to average stress results in General Postprocessor and in Timehistory Postprocessor.

For General Postprocessor the PowerGraphics module enables averaging results at all common subgrid locations except where material type discontinuities exist using APDL command *AVRES*, 2 by default [33]. In order to avoid multiple stress results for each location in a space domain one should average results at all common subgrid locations including where material type discontinuities exist using APDL command *AVRES*, 1. In this way, contour graphs of stress distribution will show the average results for locations with coincidental material, i.e. combined materials:

$$\hat{\sigma}_{av}(t) = \frac{\sum_l \sum_m \sum_n \sum_p (\hat{\sigma}(t))_{lmnp}}{N} = \frac{\hat{\sigma}(t)}{N} \quad (27)$$

where $\hat{\sigma}_{av}(t)$ is the average stress, N is a number of materials in the combined material model.

Thus to gain the "true" stress distribution the results should be multiplied by N:

$$\hat{\sigma}(t) = N\hat{\sigma}_{av}(t) \quad (28)$$

The same logic is valid for plotting graphs of stresses in Timehistory Postprocessor.

Fig. 8a and Fig. 8b represent the axial strain versus time curves for the one-dimensional one-material and two-material models for the ANSYS and analytical solutions, presented in Paragraph 3.1.

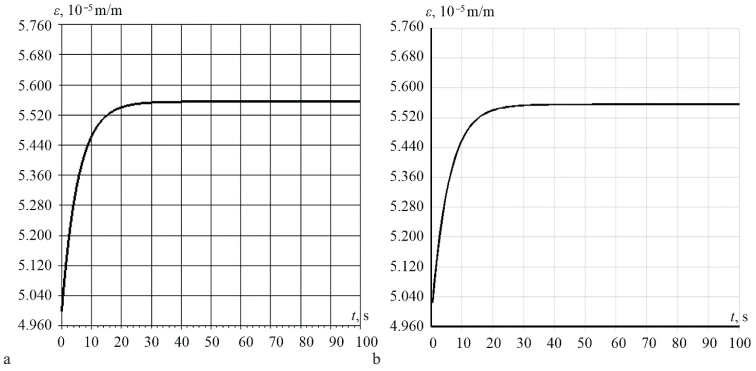

Figure 8 Axial strain versus time curves for the first and second cases of one-material model: a) analytical solution for the Wiechert model; b) numerical solution in ANSYS

In Tab. 11 the error was obtained between the results of the one–material tests and the two–material tests as well as it was performed in Paragraph 3.1 for the error between analytical and ANSYS results.

Table 11 Equivalent strains and relative errors estimation for the first two-dimensional test

Case		Strain, 10^{-5} m/m	Relative error, %
Analytical solution for the one– and two– material tests	Elastic	5.000	-
	Viscoelastic	0.556	-
	Total	5.556	-
ANSYS solution for the one–material test	Elastic	5.004	< 0.1
	Viscoelastic	0.557	< 0.1
	Total	5.561	< 0.1
ANSYS solution for the two–material test	Elastic	5.004	< 0.1
	Viscoelastic	0.558	0.4
	Total	5.562	0.1

It is unreasonable to evaluate the stress error using examples from Paragraph 3.1 and Paragraph 3.2 because in that cases the stress state is constant over the coordinates due to a constant loading. The stress error can be estimated using a contact problem of viscoelastic shells, presented below in the paper.

4. Contact problem of anisotropic viscoelasticity of a fiberglass pipe under an internal pressure and a vertical load

Let us consider a fiberglass penstock for the transportation of a corrosive media represented by a long thin cylindrical shell under an impact of an internal fluid pressure and a vertical point load contacting with an elastic foundation (Fig. 9a). The pipe is fixed in axial direction and against a rotation about axial direction at the ends that simulates abandoned parts of the pipeline system. Fig. 9b shows the finite-element model for the problem which has an element concentration in the contact region.

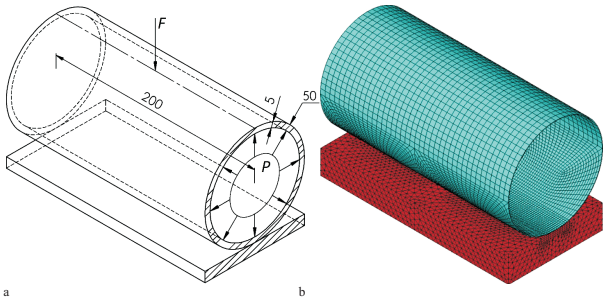

Figure 9 Models of the contact problem of viscoelastic cylindrical shell: a) calculation model (values are in millimeters, 1 mm = 10^{-3} m); b) finite-element model

The mechanical properties of fiberglass and steel, used for the problem, represent the real values approximately and are not connected with certain material grades. They are presented in Tab. 12. Steel properties were taken into account as standard values for this material that is presented in the ASTM-36 regulations [34]. The elastic orthotropic properties of fiberglass were averaged using the results of a number of publications performed in this field [35–39]. The viscoelastic properties of fiberglass were evaluated using data gained in the papers [40,41] for isotropic viscoelasticity. For the purpose of an evaluation of stress error the viscoelasticity is considered isotropic and the problem is solved using one- and two-material models.

It worth noting, that despite the fact that Fig. 9b show the finite-element model of the full model, the problem was solved using two symmetric conditions about vertical coordinate planes. Therefore, a quarter of the construction was considered.

A full value of the point load is 2000 N and a value of the pressure is 10^5 Pa. The pipe section is also subjected to the influence of the gravitation.

Fig. 10a and Fig. 10b show contour graphs of the displacement and Von Mises equivalent stress fields respectively in the construction solved for isotropic viscoelasticity using the one-material shell model for the final time 100 s. Fig. 10c and Fig. 10d show similar graphs for isotropic viscoelasticity in case of the combined two-material model. The stress field is averaged for two materials of the shell in this case. As it follows from the figures, the displacement fields coincide with a small

Table 12 Material properties for the contact problem of the shell

Material	Material parameter	Designation	Value	Unit
Steel	Elastic modulus	E_s	$2*10^{11}$	Pa
	Poisson's coefficient	ν_s	0.26	-
	Density	ρ_s	7800	kg/m^3
Fiberglass	Elastic moduli in circumferential and axial directions	E_θ, E_z	$2*10^{10}$	Pa
	Elastic modulus in radial direction	E_r	$8*10^9$	Pa
	Shear moduli between circumferential/axial and radial directions	$G_{r\theta}$, G_{rz}	$2.5*10^9$	Pa
	Shear modulus between circumferential and axial directions	$G_{\theta z}$	$1.5*10^9$	Pa
	Poisson's ratio between circumferential and axial directions	$\nu_{\theta z}$	0.3	-
	Poisson's ratio between circumferential and radial directions / axial and radial directions	$\nu_{\theta r}$, ν_{zr}	0.75	-
	Prony series multipliers	a_1 a_2 a_3 a_4	0.1 0.15 0.2 0.3	-
	Relaxation times	τ_1, τ_2, τ_3, τ_4	10, 12, 15, 20	s
	Density	ρ_f	2000	kg/m^3

error for both cases whereas the stress fields are different due to the averaging of the contour plot, depicted in Fig. 10d, as it was discussed in Paragraph 3.4.

Fig. 11a and Fig. 11b show the vertical displacement and Von Mises equivalent stress versus time curves for the location of the point load (black curves) and point, located in the opposite top end of the pipe (gray curves) for the one-material case. The analogous curves for the two-material case is identical to these ones taking into account the discussed feature of the stress distribution. They are nor presented due to a negligible error, which is evaluated below.

Table 13 presents the total displacement values and equivalent stress in the location of the point load for the one- and two-material shell models with an evaluation of errors for the two-material case in comparison with one–material one.

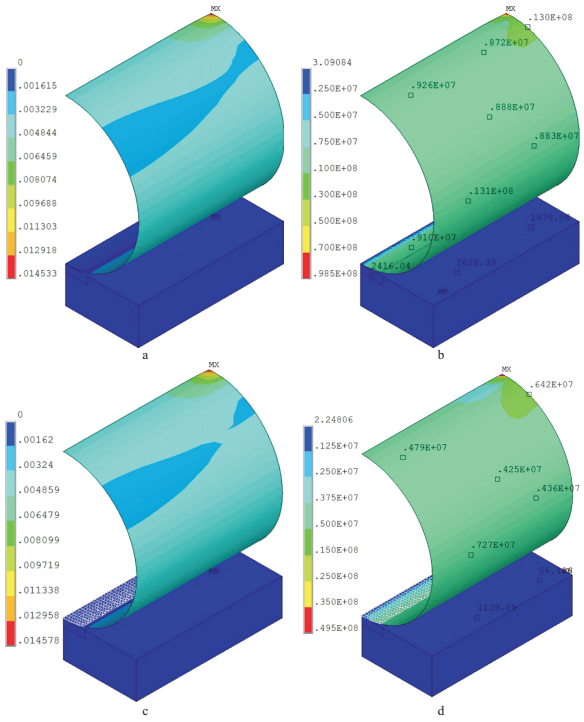

Figure 10 Finite-element model of the problem: a) total displacement distribution for the one-material shell model, [m]; b) Von Mises equivalent stress distribution for the one-material shell model, [Pa]; c) total displacement distribution for the two one-material shell model, [m]; d) Von Mises equivalent stress distribution for the two-material shell model, [Pa]

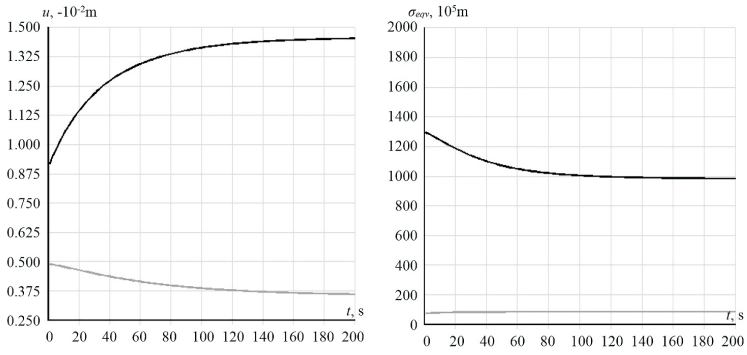

Figure 11 Dependencies on time for the contact problem of the shell: a) vertical displacement vs. time curves; (b) equivalent stress vs. time curves

Table 13 Equivalent stresses and relative errors estimation

Case		Tot. disp. 10^{-3} m	Stress 10^6 Pa	Relative error %	
				Tot. disp.	Stress
One–material ANSYS test	Elastic	9.251	129.8	-	-
	Viscoelastic	5.282	31.3	-	-
	Total	14.533	98.5	-	-
Two–material ANSYS test	Elastic	9.253	130.2	< 0.1	0.3
	Viscoelastic	5.325	31.2	0.8	0.3
	Total	14.578	99	0.3	0.5

As it follows from the table and the figures above the stress error connected with a use of the proposed combined material model is negligible and comparable with an engineering accuracy. Besides the solved problem proved an applicability of the technique to a solution of contact problems of viscoelasticity of orthotropic thin shells. This fact let us use the method in further calculations.

5. Discussion

The previous paragraph illustrated an applicability of the proposed strategy to a solution of real problems of structural mechanics but a few questions needs to be cleared in order to use it in further calculations.

5.1. *Performance of the technique*

It is obvious that an additional number of finite elements in the proposed combined material technique should increase a computational time. In order to trace the dependence of computational time on number of materials used in the combined material model let us build one-, two-, three-, four- and five-material models for the finite element problem, depictured in Fig. 5, where the end time is 100 s and a number of substeps is 200. It worth noting that the parameters for viscoelastic materials in the combined material models were gained dividing equally the viscoelastic parameters (i.e. Prony series multipliers) between these materials in each case.

The solution process was performed using ANSYS Mechanical's direct solver [42] on a Hewlett Packard Z640 Workstation with two 8-core Intel Xeon-2620 processors operating at a maximum core frequency 2.4 GHz [43] and with 128 Gb of RAM. This allowed performing a solution using the in-core memory mode [42] with 16 parallel processes.

Fig. 12 shows a dependence of a computational time on a number of materials in the combined material model.

As it follows from the diagram, the computational time increases not significantly when adding new materials to the combined material model. Thereby the proposed technique should not decrease the solution performance dramatically.

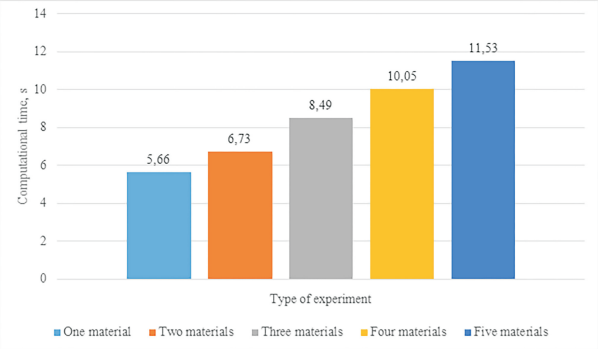

Figure 12 Computational time vs. number of materials dependence

5.2. *Multilayer option*

The mechanics of composite materials includes phenomenological and structural approaches [26]. The problems, discussed in the previous paragraphs, are based on the phenomenological approach which involves considering of the material as a homogeneous one and the physical data is gained for a series of experiments. However, the structural approach is more applicable in a lot of cases where the strength of a single layer of composite material is considered. In this case a composite shell is analyzed as a multilayer one. ANSYS Mechanical has a multilayer option for shell elements where a user is able to apply material options for each layer separately. An applicability of the proposed technique to a modeling of anisotropic viscoelasticity of certain layers of a shell may require some additional studies but however it is obvious that in case of coincidence of layers of different elements with merged nodes (i.e. equality of their layers) the method will not cause additional errors in comparison with homogeneous elements due to a linearity of the problems. Therefore, the proposed strategy is applicable to a multilayer option of shell elements.

6. Conclusion

The proposed technique allowed applying the orthotropic viscoelastic material model to the finite–element code of ANSYS Mechanical which enabled all the possibilities for solving two– and three–dimensional problems of viscoelasticity, as well as problems of homogeneous and multilayered shells. The method includes accounting of a difference in relaxation kernels and temperature shift functions for different directions. The approach was tested using one–dimensional rheological model and two-dimensional model for the plane stress case and a comparison of the results showed the sufficient accuracy of the technique. At the same time the computational performance decreases with the increasing level of anisotropy of viscoelastic material model. Thus the proposed technique is well–suitable for the problems of anisotropic viscoelasticity of thin and thick homogeneous and multilayered shells including nonlinear contact problems. Considering this the problem of contacting

of an orthotropic viscoelastic thin pipe with an elastic base was solved which proved an applicability of the method to real life problems of viscoelasticity.

Acknowledgements
The research effort was conducted at the National Technical University "Kharkiv Polytechnic Institute" within the Seventh Framework Program, Marie Curie Actions: "Innovative nondestructive testing and advanced composite repair of pipelines with volumetric surface defects", Acronym: INNOPIPES; Proposal Number: 318874; Grant Agreement Number: PIRSES-GA-2012-318874. The author would like to be obliged to National Technical University "Kharkiv Polytechnic Institute" for providing laboratory facilities.

References

[1] **Peters, S. T.**: Handbook of composites. Second edition, *Champan & Hall*, **1998**.

[2] **Ferry, J. D.**: Viscoelastic properties of polymers. Third edition, *John Wiley & Sons*, **1980**.

[3] **Christensen, R. M.**: Theory of viscoelasticity. An introduction, Academic Press, **2006**. doi:10.2307/23499350.

[4] **Roylance, D.**: Engineering Viscoelasticity, Massachusetts Institute of Technology, *Cambridge*, **2001**.

[5] ANSYS Mechanical APDL theory reference, ANSYS Inc, **2015**. http://148.204.81.206/Ansys/150/ANSYS Mechanical APDL Theory Reference.pdf

[6] Abaqus theory manual, Dassault Systems, **2010**. http://abaqusdoc.ucalgary.ca/books/stm/default.htm

[7] **Shu, L. S. and Onat, E. T.**: On anisotropic linear viscoelastic solids, *Proc. Fourth Symp. Nav. Struct. Mech., Pergamon Press*, London, 203–215, **1967**.

[8] **Taylor, Z. A., Comas, O., Cheng, M, Passenger, J., Hawkes, DJ., Atkinson, D. et al.**: On modelling of anisotropic viscoelasticity for soft tissue simulation: Numerical solution and GPU execution, *Med. Image Anal.,* 13, 234–244, **2009**. doi:10.1016/j.media.2008.10.001.

[9] **Nedjar, B.**: An anisotropic viscoelastic fibre-matrix model at finite strains: Continuum formulation and computational aspects, *Comput Methods Appl. Mech. Eng.*, 196, 1745–1756, **2007**. doi:10.1016/j.cma.2006.09.009.

[10] **Lubarda, V. and Asaro, R.**: Viscoelastic response of anisotropic biological membranes. Part II: Constitutive models, *Theor. Appl. Mech.,* 41, 213–231, **2014**. doi:10.2298/TAM1403213L.

[11] **Santos, J. E., Carcione, J. M., and Picotti, S.**:. Viscoelastic–stiffness tensor of anisotropic media from oscillatory numerical experiments, *Comput. Methods Appl. Mech. Eng.,* 200, 896–904, **2011**. doi:10.1016/j.cma.2010.11.008.

[12] **Bretin, E. and Wahab, A.**: Some anisotropic viscoelastic Green functions, *Contemp. Math,* 548, 129–148, **2011**.

[13] **Hwu, C. and Chen, Y. C.**: Analysis of defects in viscoelastic solids by a transformed boundary element method, *Procedia Eng.,* 10, 3038–3043, **2011**. doi:10.1016/j.proeng.2011.04.503.

[14] **Bai, T. and Tsvankin, I.**: Time–domain finite–difference modeling for attenuative anisotropic media, *Geophysics*, 81, 163–176, **2016**. doi:10.1190/geo2015-0424.1.

[15] **Lvov, G. I. and Martynenko, V. G.**: *Contact problem of anisotropic viscoelasticity of two cylindrical shells*, in: eds. E. Barkanov, M. Mihovski, V. Sergienko., Innov. Solut. Repair Gas Oil Pipelines, *Bulgarian Society for Non–destructive Testing Publishers*, 159–170, **2016**.

[16] **Lvov, G. I. and Martynenko, V.G.** : Development of an analytical model of a repair bandage of a pipeline, 164, 128–133, **2015**.

[17] **Poon, H. and Ahmad, M. F.**: A finite element constitutive update scheme for anisotropic, viscoelastic solids exhibiting non–linearity of the Schapery type, *Int. J. Numer. Methods Eng.,* 46, 2027–2041, **1999**. doi:10.1002/(SICI)1097-0207(19991230)46:12<2027::AID-NME575>3.0.CO;2-5.

[18] **Schapery, R. A.**: On the characterization of nonlinear viscoelastic materials, *Polym. Eng. Sci.,* 9, **1969**.

[19] **Gerngross T., Pellegrino S.**: Modelling of Anisotropic Viscoelastic Behaviour in Super-Pressure Balloons. *48th AIAA/ASME/ASCE/AHS/ASC Struct. Struct. Dyn. Mater. Conf.,* **2007**, 1–15. doi:10.2514/6.2007-1808.

[20] **Rand, J. L., Grant, D. and Strganac, T.**: The nonlinear biaxial characterization of balloon film, *34th Aerosp. Sci. Meet. Exhib.*, American Institute of Aeronautics and Astronautics, Reston, Virigina, **1996**. doi:10.2514/6.1996-574.

[21] **Rand, J. L. and Sterling, W. J.**: A constitutive equation for stratospheric balloon materials, *Adv. Sp. Res.*, 37, 2087–2091, **2006**. doi:10.1016/j.asr.2005.03.046.

[22] **Staub, S., Andrä, H., Kabel, M. and Zangmeister, T.**: Multi–scale simulation of viscoelastic fiber-reinforced composites, *Tech. Mech.*, 32, 70–83, **2012**.

[23] **Cavallini, F., Seriani, G.**: Symbolic computations in viscoelasticity and anisotropic elasticity, *8th Int. Math. Symp.,* **2006**.

[24] **Liefeith, D. and Kolling S.**: An anisotropic material model for finite rubber viscoelasticity, *LS-DYNA Adwenderforum*, Frankenthal, 25–54, **2007**.

[25] *ANSYS Mechanical APDL Introductory Tutorial,* ANSYS Inc, **2013**. http://148.204.81.206/Ansys/150/ANSYS Mechanical APDL Introductory Tutorials.pdf

[26] **Adamov, A. A., Matveenko, V. P., Trufanov, N. A., and Shardakov, I. N.**: Methods of applied viscoelasticity, UrO RAN, Ekaterinburg, **2003**.

[27] **Shinozuka, M.**: Thermorheologically simple viscoelastic materials, *AIAA J.,* 3, 375–377, **1965**. doi:10.2514/3.2870.

[28] ANSYS Mechanical APDL Material Reference, ANSYS Inc, **2013**. http://148.204.81.206/Ansys/150/APDL Material Reference.pdf

[29] ANSYS Student Products, ANSYS Inc, **2016**. http://www.ansys.com/Products/Academic/ANSYS-Student

[30] **Zhao, Y.**: Applied Maple for Engineers and Scientists, **1996**.

[31] **Nettles, A. T.**: tBasic mechanics of laminated composite plates, *NASA Ref. Publication*, 107, **1994**.

[32] **Timoshenko S, Goodier, J. N.**: Theory of elasticity, *J. Elast.*, 49, **1986**. doi:10.1007/BF00046464.

[33] ANSYS Mechanical APDL Command Reference, ANSYS Inc, **2013**. http://148.204.81.206/Ansys/150/ANSYS Mechanical APDL Command Reference.pdf

[34] A36 steel, **2016**. https://en.wikipedia.org/wiki/A36_steel

[35] **Menchawi, M. and Almgren, L.**: Modeling of fiberglass reinforced epoxy composites in LS-DYNA, **2014**.

[36] **Onuoha, F. N. and Ohanuzue, C. B. C.**: Mechanical Properties and Modeling of Fibreglass-reinforeced Epoxy Resin Wastes-filled Polypropylene, 1–8, **2014**.

[37] **Ghani, M. A. A., Salleh, Z., Hyie, K. M., Berhan, M. N., Taib, Y. M. D., and Bakri, M. A. I.**: Mechanical properties of kenaf/fiberglass polyester hybrid composite, *Procedia Eng.*, 41, 1654–1659, **2012**. doi:10.1016/j.proeng.2012.07.364.

[38] **Belaid, S., Chabira, S. F., Balland, P., Sebaa, M., and Belhouideg, S.**: Thermal aging effect on the mechanical properties of polyester fiberglass composites, 6, 2795–2803, **2015**.

[39] **Aramide, F. O., Atanda, P. O. and Olorunniwo, O. O.**: Mechanical properties of a polyester fibre glass composite, *Int. J. Compos. Mater.,* 2, 147–151, **2013**. doi:10.5923/j.cmaterials.20120206.06.

[40] **Aniskevich, K., Korsgaard, J., Mālmeisters, A. and Jansons, J.**: Creep prediction of a layered fiberglass plastic, *Mech. Compos. Mater.,* 34, 213–222, **1998**.

[41] **Kohl, J. G., Bierwisch, N., Ngo, T. T., Favaro, G., Renget, E. and Schwarzer, N.**: Determining the viscoelastic behavior of polyester fiberglass composite by continuous micro-indentation and friction properties, *Wear*, 63–67, **2016**. doi:10.1016/j.wear.2016.01.005.

[42] ANSYS Mechanical APDL Performance Guide, ANSYS Inc, **2013**.

[43] Intel Xeon Processor E5-2620 v4 (20M Cache, 2.10 GHz), Intel, **2016**. http://ark.intel.com/products/92986/Intel-Xeon-Processor- E5-2620-v4-20M-Cache-2_10-GHz